Mechanical Unfolding of an Autotransporter Passenger Protein Reveals the Secretion Starting Point and Processive Transport Intermediates

Baclayon, M.; van Ulsen, P.; Mouhib, H.; Hashemi Shabestari, M.; Verzijden, T.; Abeln, S.; Roos, W.H.; Wuite, G.J.L.

published in
ACS Nano
2016

DOI (link to publisher)
10.1021/acsnano.5b07072

document version
Early version, also known as pre-print

document license
Unspecified

Mechanical Unfolding of an Autotransporter Passenger Protein Reveals the Secretion Starting Point and Processive Transport Intermediates

Marian Baclayon,[†,‡] Peter van Ulsen,[¶] Halima Mouhib,[§] Maryam Hashemi Shabestari,[†] Timo Verzijden,[§] Sanne Abeln,[§] Wouter H. Roos,[†,‖] and Gijs J. L. Wuite[*,†]

Physics of Living Systems & LaserLaB Amsterdam, Vrije Universiteit Amsterdam, The Netherlands, , Molecular Microbiology & Amsterdam Institute for Molecules, Medicines and Systems (AIMMS), Vrije Universiteit Amsterdam, The Netherlands, Computer Science & Bioinformatics, Vrije Universiteit Amsterdam, The Netherlands, and Moleculaire Biofysica, Zernike Instituut, Rijksuniversiteit Groningen, The Netherlands

E-mail: g.j.l.wuite@vu.nl

[*]To whom correspondence should be addressed

[†]Physics of Living Systems & LaserLaB Amsterdam, Vrije Universiteit Amsterdam, The Netherlands

[‡]Present address: Bionanoscience Department, Kavli Institute of Nanoscience, TU Delft, The Netherlands

[¶]Molecular Microbiology & Amsterdam Institute for Molecules, Medicines and Systems (AIMMS), Vrije Universiteit Amsterdam, The Netherlands

[§]Computer Science & Bioinformatics, Vrije Universiteit Amsterdam, The Netherlands

[‖]Moleculaire Biofysica, Zernike Instituut, Rijksuniversiteit Groningen, The Netherlands

Abstract

The backbone of secreted autotransporter passenger proteins generally attains a stable β-helical structure. The secretion of passengers across the outer membrane was proposed to be driven by sequential folding of this structure at the cell surface. This mechanism would require a relatively-stable intermediate as starting point. Here, we investigated the mechanics of secreted truncated versions of the autotransporter Haemoglobin protease (Hbp) of *Escherichia coli* using atomic force microscopy. The data obtained reveal a β-helical structure at the C terminus that is very stable. In addition, several other distinct metastable intermediates are found which are connected during unfolding by multi-route pathways. Computational analysis indicates that these intermediates correlate to the β-helical rungs in the Hbp structure which are clamped by stacked aromatic residues. Our results suggest a secretion mechanism that is initiated by a stable C-terminal structure and driven forward by several folding intermediates that build up the β-helical backbone.

keywords: Autotransporters, Secretion, , Haemoglobin protease, AFM, Mechanical unfolding

abbreviations: AFM, atomic force microscopy; Hbp, Haemoglobin protease; IM/OM, inner/outer membrane

Classical monomeric autotransporters are a class of extracellular proteins that Gram-negative bacteria employ to interact with their environment or to invade their host. They are present in almost all the Gram-negatives and constitute the simplest bacterial secretion system to transport a protein from the cytoplasm to the cell surface.[1] Autotransporters are synthesized in the cytoplasm and contain three domains (Fig. 1): the N-terminal signal peptide, the passenger domain and the C-terminal translocation domain (β-barrel domain). The signal peptide targets the protein to the Sec machinery in the inner membrane that transports the protein to the periplasm. Then, the β-barrel

domain inserts into the outer membrane (OM) in a β-barrel conformation typical of OM-based proteins.[2] This step facilitates and initiates the OM translocation of the passenger in a concerted action with the Bam complex[3–8] (Fig. 1). After translocation of the autotransporter, the passenger domain may remain anchored to the β-barrel domain, but in most autotransporters studied to date it is proteolytically released.[1,9]

The passenger domains of autotransporters are very diverse in sequence and function but possess a conserved architecture and topology as exemplified by Haemoglobin protease (Hbp) of *Escherichia coli*. Hbp is produced by *E. coli* strains that cause intra-abdominal infection. It degrades haemoglobin and delivers heme to both *E. coli* and *Bacteroides fragilis*.[10] The structures of its passenger and β-barrel domain have been solved by X-ray crystallography[11,12] and show that the β-barrel domain folds into the typical β-barrel structure of OM-based proteins, whereas the passenger has a β-helical backbone to which functional subdomains are attached (Fig. 1). Solved crystal structures of other passenger proteins, *e.g.* of pertactin of *Bordetella pertussis*,[13] IgA1 protease of *Haemophilus influenza*[14] and VacA of *Helicobacter pylori*,[15] show a similar β-helical stem structure, with the exception of EstA of *Pseudomonas aeruginosa*,[9] whose passenger is primarily α-helical. Sequence analysis further indicated that this β-helical fold is a common feature of autotransporter passengers.[2,16,17] The prevalence of the β-helical backbone may suggest that this structure plays a crucial role in autotransporter biogenesis and transport.[1,18,19]

How the passenger domain translocates across the OM to the cell surface is under debate.[1,20,21] The β-barrel domain is thought to form a channel in the outer membrane in conjunction with the Bam complex,[3–8] and perhaps the recently described TamAB proteins.[22] Regardless of its composition, structural and mechanistic studies on the transport channel have shown that it is too narrow to translocate a fully folded passenger, or folded elements within that domain.[2,23–25] This suggests that the passenger translocates in a (partly) unfolded conformation. Furthermore, translocation of the passenger has been shown to proceed from the C to N terminus and appears independent of ATP hydrolysis or OM proton gradient.[18,23] Autotransporter mutants in which inserted cysteine pairs form a disulfide-bonded loop, preventing full secretion of the passenger, indicated that the

C-terminal region of the passenger appears first at the cell surface (Fig. 1).[23,24,26,27] In such stalled mutants the C terminus is already accessible at the cell surface. The C→N order of passenger secretion implied that it involves a hairpin configuration in the secretion channel.[1,2,19] Substitution of specific aromatic residues in the extreme C terminus by non-aromatic hydrophobic residues also blocked secretion and resulted in the formation of stalled secretion intermediates.[27,28] Such observations led to a secretion model where secretion is driven by a vectorial and processive folding of the passenger at the cell surface[1,5,18](Fig. 1). In support of such a model, it has been shown in chemical denaturation studies that the C-terminal region of the passenger is the most stable part.[17–19] Moreover, for vectorial folding to occur, one would expect that the pulling of the passenger through the translocation channel only occurs after a large folding barrier has been overcome. Increased stability of the passenger at the folding start point could provide the necessary energy to initiate this process. However, this has been difficult to assess, since folding of autotransporters in solution is not 100% efficient, suggesting that the protein does not fully refold.[17,29]

Here we identify and localize metastable substructures in Hbp by investigating the unfolding mechanics of secreted Hbp passenger variants of different lengths. We employed atomic force microscopy (AFM) for this study because it is an established and powerful technique to study intermediate protein structures.[30–33] Our results show that truncated Hbp passenger unfold *via* multi-step and multi-route pathways, with a set of distinct intermediates that show resistance to AFM-mediated unfolding. Similar patterns were observed after repetitive unfolding and refolding of the protein. By comparing the experiments to molecular dynamics simulations and computational modeling, we infer that the intermediates occur after unraveling distinct sets of rungs of the β-helix, with the rungs closest to the C terminus being the ones to unfold last. Our observations support a model in which, folding of metastable intermediate structures at the C-terminus may initiate and drive the translocation of the whole passenger across the OM.

Results and Discussion

Truncated Hbp constructs.

The crystal structure of the secreted passenger domain of Hbp (PDB: 1WXR) shows a β-helical stem-like structure of around 24 β-helices or rungs composed of two β strands (one long and one short) that form a tri-angular structure in a cross-section.[11] The functional domains are attached to this backbone, most notably a globular protease domain with a trypsin-like fold at the N terminus (Fig. 1). However, the functional domains are not pre-requisites for secretion and can be deleted.[34]

Since the prevailing model for autotransporter secretion focuses on the β-helical structure of the passenger and the role of its C terminus, we decided to study three Hbp passenger constructs: N256, A558 and L805, which represent the full-length β-helical stem (N256) and two truncated constructs (Fig. 2; all positions mentioned correspond to the full-length Hbp protein (Swiss-Prot: O88093.1)). The three constructs are efficiently secreted.[34] The shortest construct (L805) contains the first stack of six parallel β-helices after the capping β-hairpin structure at the C terminus. The hydrophobic and aromatic residues in the protein are mostly buried inside these rungs, with the aromatic rings being stacked directly on top of each other.[11] The intermediate truncated construct (A558) includes the next stack of eight β-helices, which are rotated by about 60° relative to the rungs in L805 and show less stacking of hydrophobic and aromatic residues inside. Finally the largest truncated construct N256 contains the whole of the β-helical backbone and includes the chitinase b-like functional sub-domain and the last stack of ten β-helices, which are again less well-ordered than the ones before them. It lacks the globular trypsin-like protease domain that confers the protease activity to Hbp.

To be able to attach the truncated Hbp to the AFM tip and to a gold-coated glass support, we introduced two cysteine residues into Hbp, which by itself contains no cysteine residues, by cloning a short linker at the N terminus (GSS**C**GSGSG) and by substituting the serine residue at position 967 for a cysteine residue. This residue is positioned in a loop that extends from the β-helical stem just prior to the capping structure. The truncated Hbp containing these mutations

were still efficiently secreted and could be isolated from an *E. coli* culture supernatant (Supporting Information Fig. S1).

AFM imaging and Hbp size distribution.

We first assessed whether AFM imaging of the single Hbp molecules was possible and compared the wild type Hbp passenger to the truncated constructs. The images revealed that most of the proteins adhered to the surface in an upright position when deposited onto mica (Fig. 2) which allowed us to record their height profiles and determine their size (Fig. 2C). We used mica substrates for these initial experiments to be able to determine the sizes of the Hbp proteins from the AFM imaging, because mica has a smoother surface than Au-coated glass used for pulling experiments (Supporting Information Fig. S2). The size distributions (Fig. 2E) show that the L805 and A558 constructs, which are composed mostly of β-helical rungs, were rigid with average heights of 3.6 nm and 8.1 nm, respectively. These values correspond to $1/3$ and $2/3$ of the wild type structure as solved by X-ray crystallography (13 nm, Fig. 2D).[11] The truncations appear not to disrupt the integrity of the β-helical backbone, since their sizes correspond to the expected size inferred from the crystal structures available for Hbp (1WXR[11] and 3AK5[35]). Remarkably, the N256 construct displayed a bimodal size distribution. The first peak of N256 coincides with the size of the A558 and its second peak fits closely the size of the wild type structure. Interestingly, the size distribution of the wild type Hbp passenger exhibited the same bimodal distribution as N256 (Fig. 2E, inset). These results suggest that the β-helical stack from the C terminus up to A558 forms a rigid structure, while the N-terminal region comprising the protease and chitinase sub-domains may be hinged (Fig. 1). The protein's orientation as it adheres to the surface (*i.e.* attached *via* its C or N terminus) might have revealed this structural hinge. Those attached *via* the C terminus appear with full length while those attached *via* the N terminus appear smaller because the hinged region is bent. Orientation-dependent attachment is not observed for L805 and A558, which indicates that the C-terminal β-helical stacks form a rigid structure.

AFM unfolding/refolding experiment.

To perform unfolding experiments using AFM, the cysteine-functionalized Hbp constructs (L805, A558 and N256) were deposited onto a gold-coated glass surface and approached by a gold-coated AFM tip (Fig. 2A).[30,36] Attachment and unfolding of the protein was followed by recording the force-distance curves during an approach/retract cycle of the AFM tip. A sawtooth pattern in the force-distance curve during the retract cycle signified that the protein is unfolding and, hence, that the AFM tip successfully attached to a surface-bound protein during the approach. The retraction phase could be extended to a point where the protein breaks off from the tip, or to a fixed point given by the length of the unfolded protein (0.35 nm/amino acid residue), after which a new approach/retract cycle could be started. Successive approach/retract cycles for at least 10 different L805 constructs showed that the L805 construct can reversibly unfold and refold. The protein remained attached to the tip, since during the repeated approaches the force was non-zero, which indicated that the AFM tip is under tension due to the presence of the folding protein (Fig. 3A). In the second approach, the force subsequently decreased as the tip re-approached the surface, indicating that the attached protein relaxed towards its equilibrium size. The next retraction showed a second unfolding curve, comparable to the first retraction, suggesting that the protein had refolded during the second approach. Hbp molecules typically exhibited reversible unfolding and refolding for many consecutive approach/retract cycles (Fig. 3B and Fig. 3C). The unfolding curves show that in every retraction the protein followed very similar unfolding pathways indicating that there are fixed unfolding barriers that correspond to metastable folding intermediates in the protein.

For subsequent analyses, we only considered the unfolding curves that indicated a complete unraveling of the protein (and a subsequent break off from the AFM tip). A typical full unfolding curve of an L805 construct showed multiple unfolding events, indicating the unfolding of intermediate structures within the protein (Fig. 3D). The unfolding curve was pre-processed and analyzed, for example to correct for the bending of the cantilever to which the tip is attached. Then the unfolding parameters were extracted by fitting the curve to a Worm-Like Chain (WLC) model. The WLC model has been shown to describe the elastic behavior of molecules such as DNA, RNA and

proteins[37–39] and it allowed us to characterize the unfolding barriers and determine the length of the fragments that were fully unfolded (Fig. 3E). For multiple unfolding events, the contour length (Lc) of each event corresponded to the unfolded length of a fragment (with the remainder still being folded), and indicated the position of a barrier for unfolding.

Multi-step and multi-route unfolding pathways.

The unfolding experiments revealed that the Hbp L805 construct unfolds in distinct multi-step pathways, with steps ranging from 1 to 5 and with multiple routes of unfolding in each pathway. In a 2-step pathway, the unfolding curve showed one sharp drop in force before it fully unfolded and broke from the AFM tip (Fig. 4A). The maximum forces and the fragment lengths (calculated Lc) at which these subsequent unfolding events occur are indicated by blue data points and the complete unfolding by black data points. Collectively, the recorded 2-step pathways showed that there are at least six distinct unfolding barriers in L805, which signify six relatively-stable intermediate structures, and each represented a route of unfolding. However, not every route is equally probable. Subsequent examination of the 3-step pathways (Fig. 4B) showed that again different unfolding routes exist. These routes included the same six Lc positions as found in the 2-step pathways. Overall, we observed that the L805 construct unfolds in single, two-, three-, four- or five-step pathways, with probabilities for each pathway of 20%, 42%, 25%, 10%, and 3% respectively (Supporting Information Fig. S3). Furthermore, the overall Lc distribution in these pathways revealed the presence of six metastable intermediate structures (Fig. 4C). All of the N-step pathways display fairly similar distributions of the unfolding forces with an average force of about $\sim$100 pN (Fig. 4D), which is comparable to other proteins like titin.[30] Importantly, however, the unfolding barriers at 41 nm and 47 nm are higher (median$\sim$120 pN), as compared to the other unfolding barriers (median$\sim$80 pN) (see Fig. 4D and Supporting Information Fig. S3, loading rate = 100 nm/s). Moreover, these more stable positions are also prominent in the pulling curves of L805 molecules that were repeatedly unfolded and refolded (Fig. 3C). These results, in combination with the finding that all possible routes of unfolding can be mapped onto six barriers, suggest

that this truncated construct exhibits a structured unfolding process. That is, there are sections in the protein that are weaker (Lc<40 nm) which unfold first before resistant structures (Lc>40 nm) are unfolded. Furthermore, the sizes of the unfolded fragments between the barriers are quite similar ($8 \sim 10$ nm) which suggests the unfolding of regular structures within the protein, such as the β-helices that comprise the β-helical backbone.

Computational analysis reveals N→C unraveling of the L805 β-helical backbone.

To identify which intermediate structures in the L805 protein corresponds to which unfolding barriers, we used two different computational approaches to perform this mapping on the experimentally determined Hbp structure (PDB: 1WXR).[11] Firstly, we ran two implicit solvent steered molecular dynamics (SMD) simulations to simulate unfolding of L805 under force at two different pulling rates for a total simulation time of 6 ns and 20 ns (details on the SMD simulations are described in the Supplementary Information). Secondly, we used a static model to estimate unfolding barriers by calculating the substructures that most easily unravel upon extension by force. Fig. 5A shows the resulting barriers of the SMD simulations (red and blue vertical lines, see also Table S1) and the estimated force curve from the static model (black curve), both are projected on the contour length (Lc) to make them directly comparable to the experimental data in the panels above. Both the simulations and the static model implied an N to C unfolding for L805 under the application of force and showed that N-terminal sequences appeared more prone to unfolding, while the regions of the protein resisting unfolding were located at the C terminus (Supporting Information Fig. S4 and Fig. S5). In agreement with the experimental force curves, both methods predicted two high unfolding barriers for the L805 truncated protein. These theoretically modeled peaks were mapped onto the solved crystal structure of the protein, which again indicated that the last β-helical rungs at the C terminus are the most stable part of the protein. Note that the experimentally established Lc distribution corresponds well with the simulated and modeled unfolding barriers for the more prominent peaks at the C-terminus (Fig. 5A, highlighted by the blue bands). This correspondence suggests that the highest unfolding barriers obtained from the AFM

experiment arise from the unraveling of the β-helical rungs as predicted from the calculation. This would be in consensus with a simplistic model of a sequential N→C *un*folding and in reverse of a sequential C→N folding during the secretion of Hbp, allowing the protein to pull itself through the bacterial OM. The relevant pdb structure files for each unfolding step obtained from the SMD simulations, the theoretical Lc values, and a movie of the SMD simulations to visualize the N→C unfolding are given as Supplementary Information (Supporting Information Fig. S5, Table S1 and simulation movies 1 and 2).

The positions of the unfolding barriers showed an approximate periodicity and both the simulations and static model suggested that this is due to the repetitive structure of the β-helical backbone. Furthermore, the sequences of the unfolded segments indicated that the unfolding barriers represented by the peaks at 7 and 18 nm correspond to the unfolding of the first two β-helices from the N-terminal region, followed by the unfolding of the α-helix. The hardest to unfold are the three β-helices at the C terminus, corresponding to the strong peaks calculated at 33, 39 and 47 nm. In the sequence, these unfolding barriers map to the positions of the aromatic residues that are buried inside the rungs of the β-helical backbone of Hbp that stack on top of each other (indicated in blue in Fig. 5A lowest panel and Fig. 5B). Grouping of the Lc distribution found from the AFM measurements into first, intermediate and last unfolding events revealed that all six unfolding barriers can be the first to unfold, but that the more stable barriers at Lc>40 nm are dominant among the last unfolding events. Apparently, the higher forces measured for the last two dominant unfolding barriers at 41 and 47 nm indicate that the β-helices close to the C terminus are resistant to unfolding.

Unfolding pathways of longer constructs A558 and N256.

To investigate whether sequential unfolding is also observed in the longer β-helical constructs, we also mechanically-probed the unfolding pathways of the A558 and N256 constructs by AFM and compared them to our static model (Supporting Information Fig. S6). The calculations for the N256 and A558 constructs indicated again high unfolding barriers that can be mapped to the C-terminal

protein domains (L805 section of the Hbp passenger), *i.e.* the N-terminal region should unravel first before the C-terminal part. For instance, a good match between the calculated energy peaks and the experimentally-determined Lc can be found at the 63-nm peak (Supporting Information Fig. S6C), which maps to a barrier formed by the stacked aromatic residues, F716 and F734 (gray band). This suggests that most unfolding intermediates of the measured pathways of A558 get stuck at this position before further unraveling the C-terminal part close to where L805 is located. Importantly, the last unfolding events of both N256 and A558 resemble that of the L805 Lc distribution which suggests the final unfolding of the C-terminal β-helices (Supporting Information Fig. S6C,D). These results also imply that the simple static model provided a good estimate of the unfolding pathways of the different Hbp constructs and that Hbp unfolds in domains - first to unfold are the less ordered β-helices at the N-terminal region and the last to unfold are the β-helices at the C-terminal region.

β-helices at the C terminus show resistance from unfolding.

The experimental and computational analyses show unraveling of truncated Hbp constructs in multiple steps *via* various unfolding routes. These routes were similar when the protein was probed once, or when it was allowed to refold during multiple approach/retract cycles of the AFM tip. Mechanically unfolded proteins such as titin[30] and ubiquitin,[40] often exhibit one-step unfolding for each monomeric unit of the protein. Mechanically unfolding bigger proteins revealed the presence of intermediate folding states; such as in the three-step pathways of T4 lysozyme[32] and Leucine Binding Protein (LBP),[41] bifurcated unfolding pathways of GFP,[31] and the four-intermediate unfolding states in calmodulin.[42] We find that Hbp exhibits similar unfolding behavior and displays multi-step and multi-route unfolding pathways that alternate between these intermediate states characterized by discrete unfolding barriers. However, Hbp unfolding is somehow distinct in the way that it bypasses one or several of these intermediates but the positions of the barriers remain the same. Possible reasons could be because of the repetitive nature of the structure (series of similarly-sized β-helices) or it could also indicate a definite order of unfolding.

Fig. 5C illustrates a summary of the unfolding pathways observed in the truncated Hbp L805. The metastable intermediate structures (arcs) represent the unfolding barriers in the protein that give rise to step-wise unfolding and it also shows the different routes of unfolding that the protein can take. From a folded state (center), the protein can unfold in a single step with 20% probability or in a sequential 2- to 5-step pathway with probabilities of 42%, 25%, 10% and 3%, respectively. The larger truncated constructs, N256 and A558 showed a more intricate pattern of unfolding, but in these proteins the first unfolding steps almost always mapped to the N-terminal extensions (Supporting Information Fig. S6), while the last unfolding steps showed patterns very similar to those found for L805. Furthermore, the C-terminal stable region appeared to be bordered by two stacked phenylalanine residues at positions 716 and 734, which act as distinct unfolding barriers in both proteins. Overall, the patterns suggest a high stability of the C-terminal part arising from the β-helical rungs stabilized over a ladder of aromatic residues, from which a sequential unfolding mechanism, where N-terminal passenger regions unfold prior to the C-terminal end of the passenger can be imagined. Our data also corroborates the results from chemical denaturation of pertactin and Pet autotransporter passengers,[17,19] but provides a much more detailed view on the unfolding barriers in the C-terminal region. Furthermore, the higher forces that were required to break up the β-helical structures indicates a gradient of increased stability towards the C terminus.

Stacked aromatic residues in between the β-helices form unfolding barriers.

The aromatic residues that are found buried and stacked on top of each other inside the β-helical backbone may provide stability and resistance against unfolding *via* π-π interactions.[43,44] The crystal structure of Hbp reveals that this stacking is more regular close to the C-terminus, where six aromatic residues are stacked on top of each other (Fig. 5B, bottom). Our computational analysis indicated that the dominant unfolding barriers found from AFM measurements at 41 and 47 nm result from the strong interaction between the buried aromatic residues F911 and F933, preventing the β-helices from unfolding. Stacking of additional aromatic residues on the top and bottom of F911 and F933 may further stabilize the interactions and hold the β-helical rungs together.

Apparently, the stacked aromatic residues form a stable anchor to which the rest of the β-helical backbone is built upon. This finding is in line with mutational studies that have indicated an initiating role for stacking interactions in order to fold a β-helix. For example, a high-throughput, scanning alanine mutagenesis study on the folding of the β-helical P22 tail spike[45] has shown that the stacking of hydrophobic and aromatic residues drives the processive folding of the β-helices of this structure.

A study by Soprova *et al.* on Hbp[27] has shown that mutations in the aromatic residue stack interfere with secretion. In particular, mutant W1015A (indicated in dark blue in Fig. 5B) results in a secretion block of Hbp, whereas mutant F933A resulted in a reduced secretion efficiency (Supporting Information Fig. S1C). Similar mutations of aromatic residues for the EspP and Pet passengers also resulted in either decreased secretion efficiency or a secretion block.[28,29] This suggests that the folding intermediates we report are also affected as they correspond to the structures that appear important for secretion and folding.

To further test our hypothesis, we performed unfolding experiments on a mutant of the truncated Hbp L805 construct where the phenylalanine at position 933 is substituted by alanine, L805(F933A). As expected, this mutant was clearly less well secreted as compared to the truncated Hbp L805 without mutation, but we were able to isolate enough protein material for AFM measurements (Supporting Information Fig. S1C). The AFM unfolding experiments showed that the barriers observed from the L805(F933A) construct are similar to those of L805, except for changes in the probability of their occurrence (Supporting Information Fig. S7A). In particular, the probability of unfolding at the most resistant barrier at 47 nm (Supporting Information Fig. S7B) is now much higher when compared to L805, which suggests a stabilizing role of F933 for the structures close to the C terminus of the passenger in the wild type Hbp. This result is in line with our model, because it is this barrier (Lc$\sim$47 nm) that we associated with residue F933 in the simulation and the computational model (see mapping of the residues relative to the Lc, bottom plot in Fig. 5A). We can also compare the unfolding forces involved for the two constructs. For L805 the forces needed to unfold the weaker barrier (Lc<25 nm) were a factor of $\sim$1.5 lower than

the final two barriers close to the C terminus. For the mutant on the other hand, it seems that all barriers unfold at more or less the same force. Together, these data of the mutant confirm our idea that the strong intermediate states seen in L805 can indeed be mapped onto the C-terminal area of the passenger.

Initiation of C→N folding of the Hbp passenger during secretion

The majority of natural autotransporter passengers are predicted to form parallel β-helices.[1,16,17] The combined observations of the secretion pore size,[25] which is too narrow for fully folded passengers, and of the C-terminal part of the passenger appearing first at the cell surface[23] led to a secretion model where processive extracellular folding drives the secretion (reviewed in,[1] Fig. 1). The detailed multi-step unfolding pathway of Hbp as probed by AFM and two different computational analysis methods show clear unfolding barriers which could be mapped onto the β-helical rungs of the C-terminal domain of Hbp, and suggest a possible mechanism how the secretion process is initiated: the unfolding seems to progress along distinct intermediate steps, with the C-terminal rungs of the β-helix being the most stable and last to unfold. These last two β-helical rungs require a distinctly higher force to unfold. Notably that stability can be abolished by a deletion of a single phenylalanine between these two last β-helical rungs. The last step involving the unfolding of the stable C-terminal rungs is also found in the larger constructs A558 and N256, which showed unfolding routes that invariably appeared to end at the C-terminal β-helical rungs. Overall, the order of steps and the applied forces necessary to overcome the unfolding barriers involved, supports the hypothesis that the Hbp folding pathway is sequential. This folding of Hbp from C→N may explain how the protein is able to pull itself through the bacterial OM without further assistance from its surroundings. Finally, our results further suggest that the stacking of the aromatic residues is the main driver for the initiation of processive folding of Hbp from the C-terminal β-helices onwards.

Conclusion

Combining our observations with literature, we suggest the following autotransporter secretion mechanism: translocation starts with the insertion of a hairpin into the β-barrel domain, while it is assembled by the Bam complex in the OM. This exposes the first β-strands of the passenger on the bacterial surface. From here the folding of the β-helical backbone progresses and becomes more energetically-favorable due to the π-π stacking of the aromatic rings. That is, the energy to pull the first β-helices across the OM is compensated for by the formation of the aromatic ladder during the very first stage of the passenger folding. The folded protein is stabilized by the hydrophobic core of the β-helical backbone. Our results further suggest that the processive folding could follow multiple routes, jumping between different folding barriers, which explains why mutations located outside of the C-terminal β-helical core that affect the overall passenger stability have only a minor influence on secretion and processive folding.[46] While natural or recombinant non-β-helical passengers exist[1,9,47,48] and alternative secretion mechanisms have been proposed,[21,48] also in these cases the folding of an initial C-terminal segment *via* intra-molecular or even inter-molecular interactions is proposed as an important first step for secretion. To conclude, our experimental and computational unfolding results show high unfolding barriers located at the C terminus of the secreted Hbp passenger, which can be mapped to the β-helical rungs in this domain. This implies that this C-terminal domain is the most stable part of the secreted protein and the most difficult to unfold. Our results suggest that the energy provided by the sequential folding of the C-terminal domain may be the driving force during the secretion of Hbp across the bacterial OM, supporting a vectorial-folding mechanism at least in initiating the secretion of these proteins.[1,5,18]

Methods

Hbp Cloning

The cloning of the truncated constructs and the secretion of the resulting passengers has been described earlier by Jong *et al.*[34] In all constructs the truncated passengers are preceded by the short linker GSS**C**GSGSG. The linker contains a cysteine residue that serves as a handle at the N terminus for the AFM experiments. To include a similar Cys-residue handle in the C-terminal part of the passenger, a cysteine was engineered at position 967 of the passenger, substituting the serine residue at that position. The cloning involved a three-primer PCR strategy using Phusion DNA polymerase (Finnzymes).

In a first PCR reaction, primers Hbp-mut S967C (5'-CAAGCGTGTCCTTGTTACAAGGTTTT-3') and pEH3-Rev (5'-GTGAATTCGGATCCAGAGATGTGT-3') were combined with pEH3-Hbp plasmid as DNA template.[24] The resulting amplicon was purified by gel extraction (Qiagen) and used in a second PCR in combination with primer Hbp-KpnI-F (CGGGTACCGCAATATCTGGA) and vector pEH3-Hbp as a template. The resulting amplicon was cloned into the vectors that encoded the truncated Hbp using restriction enzymes KpnI and EcoRI. The resulting plasmids were checked by sequencing for the presence of the mutation that results in the S967C substitution.

The plasmid encoding the Hbp-L805(F933A) mutant was made by using a similar three-primer strategy, but using primers N-W933A-f[27] and pEH3-Rev in the first PCR and the resulting fragment and Hbp-KpnI-F in the second PCR to introduce the substitution of the phenylalanine at position 933 for alanine.

Atomic Force Microscopy

The measurements were performed on a Bruker BioCatalyst AFM and conducted in liquid using the Peak Force Tapping mode. For imaging, SiN cantilever tips (Olympus OMCL-RC800PSA) with nominal spring constants of 50 pN/nm were used. The Hbp samples were diluted in 5 mM Tris + 5 mM $MgCl_2$ buffer solution and deposited onto the surface of a freshly-cleaved mica. For

unfolding experiments, SiN cantilevers with Au-coated tips (Olympus BL-RC-150VB-C1) and nominal spring constants of 30 pN/nm were used. These cantilevers were calibrated using the thermal tuning method.[49] The Hbp samples were diluted in 50 μL PBS buffer at pH 7 to a concentration of 1$\sim$2 mg/mL and incubated onto an Au-coated glass cover slip. The proteins were immobilized on the surface through the covalent Au-S bonding between the gold surface and cysteine handles, and thoroughly washed-off for any unbound proteins.[50,51] Data on the unfolding of Hbp was collected by the AFM, which performed 10 to 20 approach/retract cycles at each xy position (spaced at least 25 nm apart so as not to pull the same protein molecule). This yielded an efficiency of detecting an unfolding event of about 5%, although only about 1% resulted to full-length unfolding of the protein. The unfolding lengths and forces involved was deduced from the force-distance curves of the protein during the retract cycles. These curves were first processed (offsetting and deleting the baseline and the section where the tip made contact with the surface) and corrected for the cantilever-bending as illustrated in Fig. 3D. The cantilever bending correction is done by transforming the x-axis to $x_{unfold} = x_{retract} - F/k$, where F and k are the measured force and the spring constant of the cantilever, respectively. The unfolding curve displays multiple discontinuities as the protein is unraveled. These discontinuities refer to the step-wise unfolding of protein fragments, which are delimited by local unfolding barriers that are hard to unravel. The unfolding of a fragment is defined when a discontinuity is recorded with a force drop of $>$50 pN. Each fragment is then fitted with the Worm-Like Chain (WLC) model $F = (k_B T)/L_p[1/4(1-x/L_c)^{-2} + x/L_c - 1/4]$, where k_B, T, L_p and L_c are the Boltzmann's constant, temperature, persistence and contour lengths of the protein, respectively (Fig. 3E).

Static Model and Molecular Dynamics Simulations

In the static model, the free energies of unfolding specific fragments of Hbp were estimated based upon the number of contacts and hydrogen bonds to be broken when the Hbp crystal is taken into account. Two residues were considered to make a contact if their C_β atoms lie within 0.7 nm of each other, while the pairwise hydrogen bonds in the peptide backbone were assigned by the

DSSP program based on the given PDB structure (PDB: 1WXR).[52] A computational approach was performed that took into account the number of contacts and hydrogen bonds broken during unfolding to search for metastable intermediate structures in the different Hbp constructs.

To reconstruct and understand the AFM experiment at a molecular scale, full-atomistic Steered Molecular Dynamics (SMD) simulations were carried out on the truncated L805 construct of wild type Hbp. The SMD simulations were carried out at a full-atomistic level using an implicit water model (GBSA)[53] and the AMBER99SB-ILDN force field[54] using a time step of 2 fs at constant pulling rates of 0.01 nm/ps and 0.003 nm/ps for the 6 ns and the 20 ns simulation and a spring constant of 1000 kJ/mol·nm^2, respectively. All simulations were carried out using the GROMACS 4.5.5 program package.[55]

Acknowledgement

This work was supported by a STW-administered NanoSci-E+ Grant (to G.J.L.W), a STW-HTSM grant (to W.H.R. and G.J.L.W.), the NanoNextNL consortium of the Dutch Government and partners (to G.J.L.W), a VIDI grant of the Nederlandse Organisatie voor Wetenschappelijk Onderzoek (NWO) (to W.H.R.), a VICI grant of NWO (to G.J.L.W), an EMBO short-term fellowship (to H. M.) and a VCI grant (Verband der Chemischen Industrie e.V.) to finance the workstation for the SMD simulations ('Sachkostenzuschuss für den Hochschulnachwuchs' to H.M.).

Supporting Information Available: Details of the experimental methods, AFM analyses, static modeling and molecular simulations. This material is available free of charge *via* the Internet at http://pubs.acs.org.

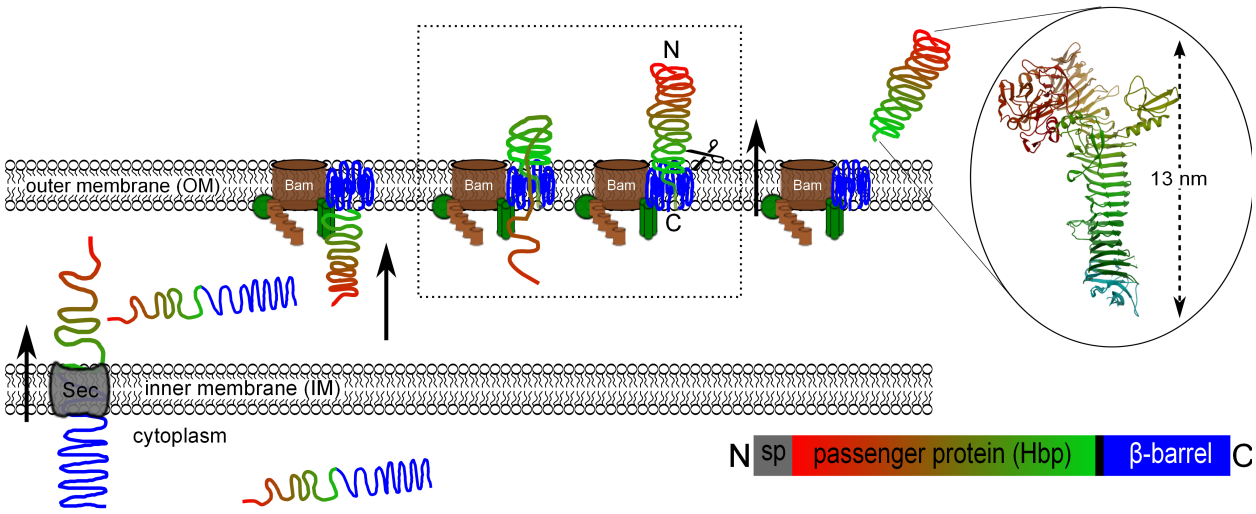

Figure 1: **S**ecretion model of the autotransporter system. Autotransporters are secreted in two steps, across the inner and outer membranes (IM/OM). Autotransporters are composed of three domains: the N-terminal signal peptide (sp), the passenger domain and the β-barrel domain. Its secretion across the IM is facilitated by the Sec machinery, and its secretion across the OM is hypothesized to be a folding-driven process assisted by the Bam complex (dotted box). A cartoon representation of the solved crystal structure of the 1048-residue passenger domain of Hbp is shown in circle.[11] The C-terminal part of the passenger (indicated in cyan) is thought to appear first at the cell surface. The Hbp passenger domain has a long β-helical backbone comprising 24 rungs of β-helices (green) with an end-to-end length of 13 nm. The passenger C terminus contains a partly disordered cap region and includes the first β-helix (cyan). The following 14 β-helices are quite regular and have a core that is filled with hydrophobic and aromatic residues (Trp and Phe), of which the first five are stacked on top of each other and on top of the W1015 in the cap region. At the N terminus a chitinase-like and a protease domain extend from the β-helical backbone.

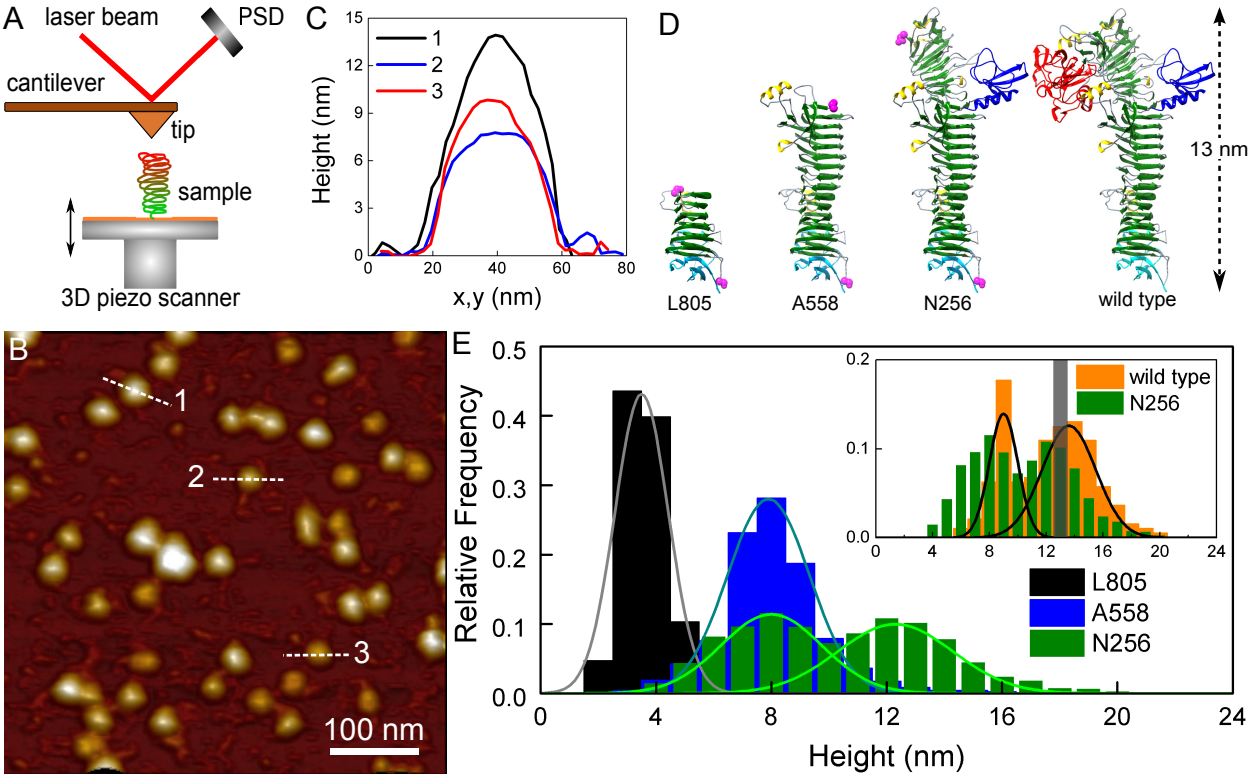

Figure 2: **A**FM imaging and protein size distribution. (A) Schematic diagram of an AFM. (B) AFM image of Hbp wild-type sample on mica and (C) their height profiles.(D) Cartoon models of the assumed structures of the truncated Hbp based on the solved structure of the wild type Hbp. Protein domains: C-terminal cap region (cyan), β-helical backbone (green), chitinase b-like domain (blue), α-helices (yellow), serine protease domain (red) and cysteine handles (magenta). (E), The size distributions for the truncated Hbp constructs as measured by AFM. Inset: Comparison of the size distribution of the truncated Hbp construct N256 and wild type Hbp. The size of the wild type Hbp according to the solved X-ray structure is indicated by the gray band at 13 nm. PSD: Position Sensitive Detector

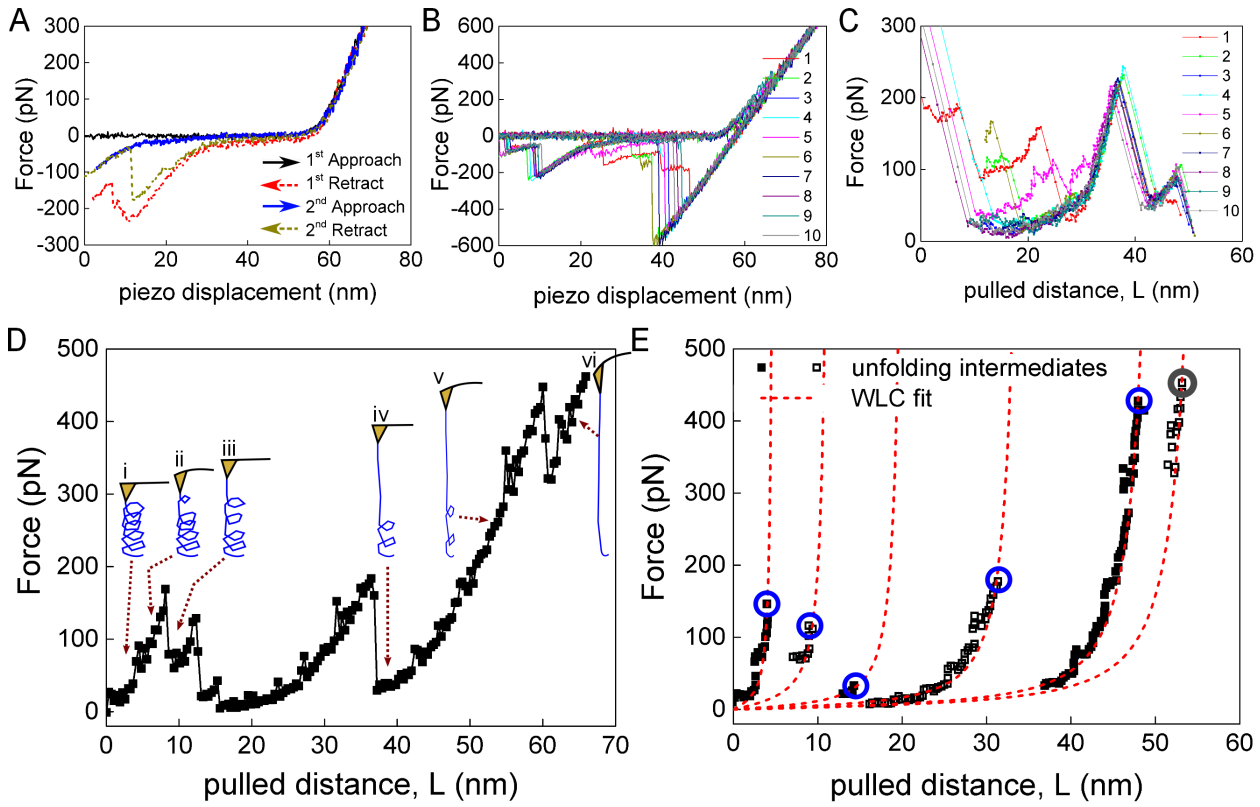

Figure 3: **U**nfolding force-distance curves. (A) 2 and (B) 10 successive approach and retract cycles showing reversible folding and unfolding of single L805 truncated Hbp. (C) Unfolding curves in (B), showing two strong barriers as well as weak ones that are stochastically probed during the refolding/unfolding cycles. (D) An example of a complete unfolding of a single L805 construct with illustrations on how the protein molecule stretches and unfolds, and the corresponding cantilever bending. The force is gradually increasing as the protein is being stretched (i, ii, v, vi) and drops sharply as a fragment is unfolded (iii, iv). (E), The unfolding curve in (D) is corrected for the cantilever bending, yielding the unfolding characteristics due to the protein alone. The maximum force in unfolding a fragment is indicated by blue circles, and the complete unraveling and break-off from the AFM tip by a gray circle. To determine the unfolded length of the intermediates (contour length, Lc), each unfolding fragment is fitted with a Worm-Like Chain (WLC) model with a persistence length, Lp of 0.4 nm, a typical value for proteins (red broken lines).

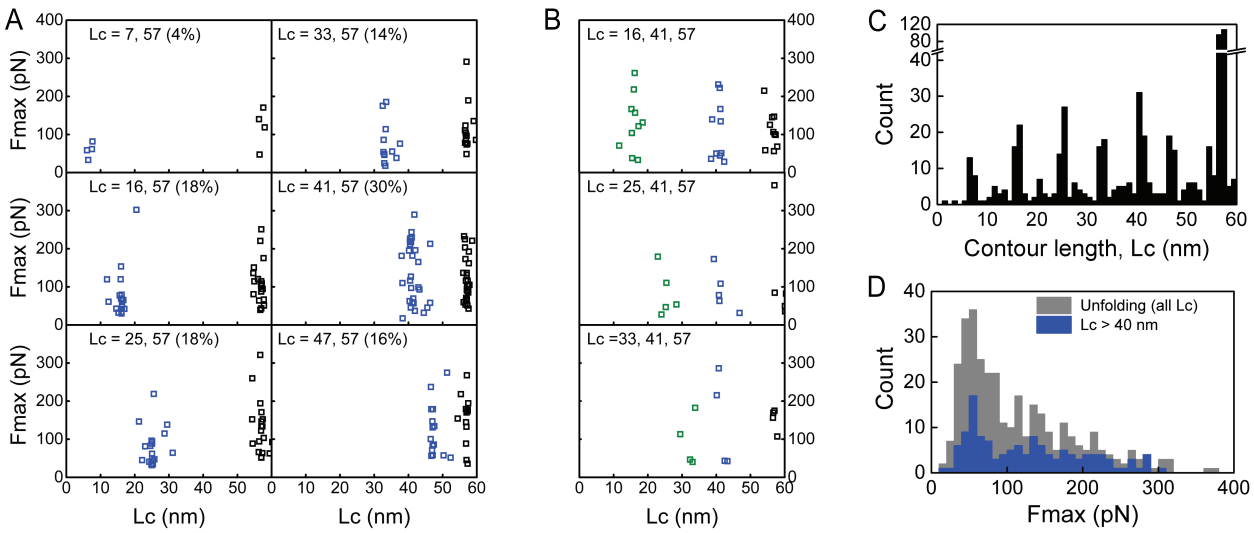

Figure 4: **M**ulti-step and multi-route unfolding pathways of the truncated Hbp construct L805. Routes for the (A) 2-step pathways collected from the complete unfolding curves of 120 individual L805 molecules, showing six unfolding intermediates. (B) Selected 3-step unfolding pathways with intermediate unfolding at Lc = 41 nm. (C) The contour length distribution of the unfolded fragments for all n-step unfolding pathways. There are six dominating unfolding barriers at 7, 16, 25, 33, 41 and 47 nm before the L805 construct is fully unraveled at around 58 nm. (D) The maximum unfolding force distribution, showing similar distribution for all n-step unfolding pathways, except that the unfolding barriers at Lc>40 nm record higher unfolding forces.

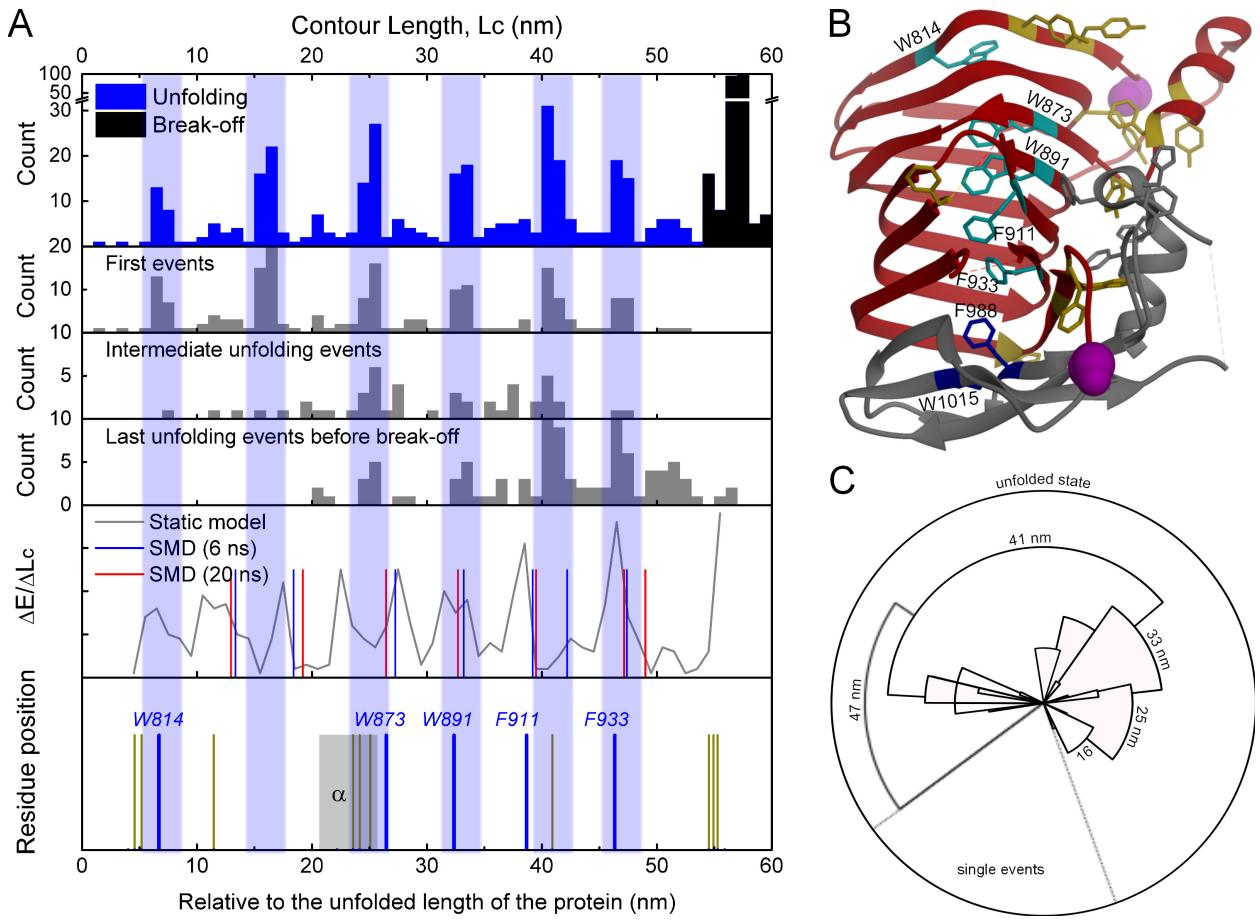

Figure 5: **C**omparison between experiment and calculation. (A) Positions of the aromatic residues in the protein sequence, unfolding barriers found from the calculation and the histograms of the measured contour lengths from the AFM mechanical unfolding experiments. (B) The structure of L805 construct showing the stack of 7 aromatic residues (in cyan and blue) buried inside the β-helical backbone. The other aromatic residues are in yellow, while the cysteine handles are in magenta. The relative positions of the residues are also drawn in the same color as in (A). The calculated unfolding barriers in (A) largely coincide with the experiment as highlighted by the blue bands. The calculation shows that the barriers correspond to the positions of aromatic residues that are buried and stacked inside the β-helical loops (blue lines). The intermediate unfolding events show that the six barriers are unfolded first with similar probability (25%), but the 41 and 47 nm are the most dominant last unfolding barriers before the protein is completely unraveled and broke-off from the AFM tip. (C) Representation of the unfolding landscape of the Hbp L805 construct. The radius represents the position of the unfolding barrier, the angle of the arc represents the probability of encountering the unfolding barrier, and the center and outer diameter represent the protein's folded and unfolded configurations, respectively. The radial lines represent the different routes of unfolding.

References

1. van Ulsen, P.; Rahman, S. U.; Jong, W. S. P.; Daleke-Schermerhom, M. H.; Luirink, J. Type V Secretion: From Biogenesis to Biotechnology. *Biochim. Biophys. Acta, Mol. Cell Res.* **2014**, *1843*, 1592–1611.

2. Oomen, C.; van Ulsen, P.; Van Gelder, P.; Feijen, M.; Tommassen, J.; Gros, P. Structure of the Translocator Domain of a Bacterial Autotransporter. *EMBO J.* **2004**, *23*, 1257–1266.

3. Sauri, A.; Oreshkova, N.; Soprova, Z.; Jong, W. S. P.; Sani, M.; Peters, P. J.; Luirink, J.; van Ulsen, P. Autotransporter Beta-Domains Have a Specific Function in Protein Secretion beyond Outer-Membrane Targeting. *J. Mol. Biol.* **2011**, *412*, 553–567.

4. Ieva, R.; Tian, P.; Peterson, J. H.; Bernstein, H. D. Sequential and Spatially Restricted Interactions of Assembly Factors with an Autotransporter Beta Domain. *Proc. Natl. Acad. Sci. U. S. A.* **2011**, *108*, E383–E391.

5. Pavlova, O.; Peterson, J. H.; Ieva, R.; Bernstein, H. D. Mechanistic Link between Beta Barrel Assembly and the Initiation of Autotransporter Secretion. *Proc. Natl. Acad. Sci. U. S. A.* **2013**, *110*, E938–E947.

6. Sauri, A.; Soprova, Z.; Wickstrom, D.; de Gier, J.-W.; Van der Schors, R. C.; Smit, A. B.; Jong, W. S. P.; Luirink, J. The Bam (Omp85) Complex is Involved in Secretion of the Autotransporter Haemoglobin Protease. *Microbiology* **2009**, *155*, 3982–3991.

7. Ieva, R.; Bernstein, H. D. Interaction of an Autotransporter Passenger Domain with BamA During its Translocation Across the Bacterial Outer Membrane. *Proc. Natl. Acad. Sci. U. S. A.* **2009**, *106*, 19120–19125.

8. Ricci, D. P.; Hagan, C. L.; Kahne, D.; Silhavy, T. J. Activation of the Escherichia coli Beta-Barrel Assembly Machine (Bam) is Required for Essential Components to Interact Properly with Substrate. *Proc. Natl. Acad. Sci. U. S. A.* **2012**, *109*, 3487–3491.

9. van den Berg, B. Crystal Structure of a Full-Length Autotransporter. *J. Mol. Biol.* **2010**, *396*, 627–633.

10. Otto, B.; van Dooren, S.; Nuijens, J.; Luirink, J.; Oudega, B. Characterization of a Hemoglobin Protease Secreted by the Pathogenic Escherichia coli Strain EB1. *J. Exp. Med.* **1998**, *188*, 1091–1103.

11. Otto, B.; Sijbrandi, R.; Luirink, J.; Oudega, B.; Heddle, J.; Mizutani, K.; Park, S.; Tame, J. Crystal Structure of Hemoglobin Protease, a Heme Binding Autotransporter Protein from Pathogenic Escherichia coli. *J. Biol. Chem.* **2005**, *280*, 17339–17345.

12. Tajima, N.; Kawai, F.; Park, S.-Y.; Tame, J. R. H. A Novel Intein-Like Autoproteolytic Mechanism in Autotransporter Proteins. *J. Mol. Biol.* **2010**, *402*, 645–656.

13. Emsley, P.; Charles, I.; Fairweather, N.; Isaacs, N. Structure of Bordetella pertussis virulence factor P.69 pertactin. *Nature* **1996**, *381*, 90–92.

14. Johnson, T. A.; Qiu, J.; Plaut, A. G.; Holyoak, T. Active-Site Gating Regulates Substrate Selectivity in a Chymotrypsin-Like Serine Protease: The Structure of Haemophilus influenzae Immunoglobulin A1 Protease. *J. Mol. Biol.* **2009**, *389*, 559–574.

15. Gangwer, K. A.; Mushrush, D. J.; Stauff, D. L.; Spiller, B.; McClain, M. S.; Cover, T. L.; Lacy, D. B. Crystal structure of the Helicobacter pylori vacuolating toxin p55 domain. *Proc. Natl. Acad. Sci. USA* **2007**, *104*, 16293–16298.

16. Kajava, A. V.; Steven, A. C. The Turn of the Screw: Variations of the Abundant Beta-Solenoid Motif in Passenger Domains of Type V Secretory Proteins. *J. Struct. Biol.* **2006**, *155*, 306–315, 4th Workshop on Coiled Coils, Collagen and Co-Proteins, Alpbach, Austria, Sep 11-17, 2005.

17. Junker, M.; Schuster, C.; McDonnell, A.; Sorg, K.; Finn, M.; Berger, B.; Clark, P. Pertactin Beta-Helix Folding Mechanism Suggests Common Themes for the Secretion and Folding of Autotransporter Proteins. *Proc. Natl. Acad. Sci. U. S. A.* **2006**, *103*, 4918–4923.

18. Braselmann, E.; Clark, P. L. Autotransporters: The Cellular Environment Reshapes a Folding Mechanism to Promote Protein Transport. *J. Phys. Chem. Lett.* **2012**, *3*, 1063–1071.

19. Renn, J. P.; Clark, P. L. A Conserved Stable Core Structure in the Passenger Domain Beta-Helix of Autotransporter Virulence Proteins. *Biopolymers* **2008**, *89*, 420–427.

20. Bernstein, H. D. Looks can be Deceiving: Recent Insights into the Mechanism of Protein Secretion by the Autotransporter Pathway. *Mol. Microbiol.* **2015**, *97*, 205–215.

21. Drobnak, I.; Braselmann, E.; Clark, P. L. Multiple Driving Forces Required for Efficient Secretion of Autotransporter Virulence Proteins. *J. Biol. Chem.* **2015**, *290*, 10104–10116.

22. Selkrig, J.; Mosbahi, K.; Webb, C. T.; Belousoff, M. J.; Perry, A. J.; Wells, T. J.; Morris, F.; Leyton, D. L.; Totsika, M.; Phan, M.-D. et al. Discovery of an archetypal protein transport system in bacterial outer membranes. *Nature Structural & Molecular Biology* **2012**, *19*, 506–U63.

23. Junker, M.; Besingi, R. N.; Clark, P. L. Vectorial Transport and Folding of an Autotransporter Virulence Protein During Outer Membrane Secretion. *Mol. Microbiol.* **2009**, *71*, 1323–1332.

24. Jong, W. S. P.; ten Hagen-Jongman, C. M.; den Blaauwen, T.; Slotboom, D. J.; Tame, J. R. H.; Wickstrom, D.; de Gier, J.-W.; Otto, B. R.; Luirink, J. Limited Tolerance Towards Folded Elements During Secretion of the Autotransporter Hbp. *Mol. Microbiol.* **2007**, *63*, 1524–1536.

25. Sauri, A.; ten Hagen-Jongman, C. M.; van Ulsen, P.; Luirink, J. Estimating the Size of the Active Translocation Pore of an Autotransporter. *J. Mol. Biol.* **2012**, *416*, 335–345.

26. Oliver, D.; Huang, G.; Nodel, E.; Pleasance, S.; Fernandez, R. A conserved region within the Bordetella pertussis autotransporter BrkA is necessary for folding of its passenger domain. *Molecular Microbiology* **2003**, *47*, 1367–1383.

27. Soprova, Z.; Sauri, A.; van Ulsen, P.; Tame, J. R. H.; den Blaauwen, T.; Jong, W. S. P.; Luirink, J. A Conserved Aromatic Residue in the Autochaperone Domain of the Autotrans-

porter Hbp Is Critical for Initiation of Outer Membrane Translocation. *J. Biol. Chem.* **2010**, *285*, 38224–38233.

28. Peterson, J. H.; Tian, P.; Ieva, R.; Dautin, N.; Bernstein, H. D. Secretion of a Bacterial Virulence Factor is Driven by the Folding of a C-Terminal Segment. *Proc. Natl. Acad. Sci. U. S. A.* **2010**, *107*, 17739–17744.

29. Renn, J. P.; Clark, P. L. In *Methods in Enzymology: Biothermodynamics*; Johnson M. L., Holt J. M. and Ackers G. K.,, Ed.; Methods in Enzymology; Elsevier Academic Press Inc, 2011; Vol. 492; pp 233–251.

30. Rief, M.; Gautel, M.; Oesterhelt, F.; Fernandez, J. M.; Gaub, H. E. Reversible Unfolding of Individual Titin Immunoglobulin Domains by AFM. *Science* **1997**, *276*, 1109–1112.

31. Mickler, M.; Dima, R. I.; Dietz, H.; Hyeon, C.; Thirumalai, D.; Rief, M. Revealing the Bifurcation in the Unfolding Pathways of GFP by using Single-Molecule Experiments and Simulations. *Proc. Natl. Acad. Sci. U. S. A.* **2007**, *104*, 20268–20273.

32. Peng, Q.; Li, H. Atomic Force Microscopy Reveals Parallel Mechanical Unfolding Pathways of T4 Lysozyme: Evidence for a Kinetic Partitioning Mechanism. *Proc. Natl. Acad. Sci. U. S. A.* **2008**, *105*, 1885–1890.

33. Junker, J. P.; Ziegler, F.; Rief, M. Ligand-Dependent Equilibrium Fluctuations of Single Calmodulin Molecules. *Science* **2009**, *323*, 633–637.

34. Jong, W. S. P.; Soprova, Z.; de Punder, K.; ten Hagen-Jongman, C. M.; Wagner, S.; Wickstrom, D.; de Gier, J.-W.; Andersen, P.; van der Wel, N. N.; Luirink, J. A Structurally Informed Autotransporter Platform for Efficient Heterologous Protein Secretion and Display. *Microb. Cell Fact.* **2012**, *11*.

35. Nishimura, K.; Tajima, N.; Yoon, Y.-H.; Park, S.-Y.; Tame, J. R. H. Autotransporter Passenger

Proteins: Virulence Factors with Common Structural Themes. *J. Mol. Med.* **2010**, *88*, 451–458.

36. Baclayon, M.; Roos, W. H.; Wuite, G. J. L. Sampling Protein Form and Function with the Atomic Force Microscope. *Mol. Cell. Proteomics* **2010**, *9*, 1678–1688.

37. Bustamante, C.; Marko, J.; Siggia, E.; Smith, S. Entropic Elasticity of Lambda-Phage DNA. *Science* **1994**, *265*, 1599–1600.

38. Kumar, S.; Li, M. S. Biomolecules under Mechanical Force. *Phys. Rep.* **2010**, *486*, 1–74.

39. Staple, D. B.; Payne, S. H.; Reddin, A. L. C.; Kreuzer, H. J. Stretching and Unfolding of Multidomain Biopolymers: a Statistical Mechanics Theory of Titin. *Phys. Biol.* **2009**, *6*.

40. Chyan, C.; Lin, F.; Peng, H.; Yuan, J.; Chang, C.; Lin, S.; Yangy, G. Reversible Mechanical Unfolding of Single Ubiquitin Molecules. *Biophys. J.* **2004**, *87*, 3995–4006.

41. Kotamarthi, H. C.; Sharma, R.; Narayan, S.; Ray, S.; Ainavarapu, S. R. K. Multiple Unfolding Pathways of Leucine Binding Protein (LBP) Probed by Single-Molecule Force Spectroscopy (SMFS). *J. Am. Chem. Soc.* **2013**, *135*, 14768–14774.

42. Stigler, J.; Ziegler, F.; Gieseke, A.; Gebhardt, J. C. M.; Rief, M. The Complex Folding Network of Single Calmodulin Molecules. *Science* **2011**, *334*, 512–516.

43. Meyer, E.; Castellano, R.; Diederich, F. Interactions with Aromatic Rings in Chemical and Biological Recognition. *Angew. Chem., Int. Ed.* **2003**, *42*, 1210–1250.

44. Kong, F.; King, J. Contributions of Aromatic Pairs to the Folding and Stability of Long-Lived Human Gamma D-Crystallin. *Protein Sci.* **2011**, *20*, 513–528.

45. Simkovsky, R.; King, J. An Elongated Spine of Buried Core Residues Necessary for *In Vivo* Folding of the Parallel Beta-Helix of P22 Tailspike Adhesin. *Proc. Natl. Acad. Sci. U. S. A.* **2006**, *103*, 3575–3580.

46. Kang'ethe, W.; Bernstein, H. D. Stepwise Folding of an Autotransporter Passenger Domain is Not Essential for its Secretion. *J. Biol. Chem.* **2013**, *288*, 35028–35038.

47. Besingi, R. N.; Chaney, J. L.; Clark, P. L. An alternative Outer Membrane Secretion Mechanism for an Autotransporter Protein Lacking a C-Terminal Stable Core. *Mol. Microbiol.* **2013**, *90*, 1028–1045.

48. Kang'ethe, W.; Bernstein, H. D. Charge-Dependent Secretion of an Intrinsically Disordered Protein *via* the Autotransporter Pathway. *Proc. Natl. Acad. Sci. U. S. A.* **2013**, *110*, E4246–E4255.

49. Hutter, J. L.; Bechhoefer, J. Calibration of Atomic Force Microscope Tips. *Rev. Sci. Instrum.* **1993**, *64*, 1868–1873.

50. Ebner, A.; Wildling, L.; Zhu, R.; Rankl, C.; Haselgrubler, T.; Hinterdorfer, P.; Gruber, H. J. *STM and AFM Studies on*; Topics in Current Chemistry; Springer-Verlag Berlin: Berlin, 2008; Vol. 285; pp 29–76.

51. Ferrero, V. E. V.; Andolfi, L.; Di Nardo, G.; Sadeghi, S. J.; Fantuzzi, A.; Cannistraro, S.; Gilardi, G. Protein and Electrode Engineering for the Covalent Immobilization of P450 BMP on Gold. *Anal. Chem.* **2008**, *80*, 8438–8446.

52. Kabsch, W.; Sander, C. Dictionary of Protein Secondary Structure: Pattern Recognition of Hydrogen-Bonded and Geometrical Features. *Biopolymers* **1983**, *22*, 2577–2637.

53. Onufriev, A.; Bashford, D.; Case, D. Exploring Protein Native States and Large-Scale Conformational Changes with a Modified Generalized Born Model. *Proteins: Struct., Funct., Bioinf.* **2004**, *55*, 383–394.

54. Hornak, V.; Abel, R.; Okur, A.; Strockbine, B.; Roitberg, A.; Simmerling, C. Comparison of Multiple Amber Force Fields and Development of Improved Protein Backbone Parameters. *Proteins: Struct., Funct., Bioinf.* **2006**, *65*, 712–725.

55. Van der Spoel, D.; Lindahl, E.; Hess, B.; Groenhof, G.; Mark, A.; Berendsen, H. GROMACS: Fast, Flexible, and Free. *J. Comput. Chem.* **2005**, *26*, 1701–1718.

Graphical TOC Entry